DESIGN AND CHARACTERIZATION OF A SUPERSONIC WIND TUNNEL

FOR THE

STUDY OF SHOCK WAVE BOUNDARY LAYER INTERACTIONS

A THESIS

Presented in Partial Fulfillment of the Requirements for Graduation with Distinction in the Department of Mechanical Engineering at The Ohio State University

By

Christopher J. Clifford

.....

The Ohio State University

2010

ABSTRACT

A new 3”x3” supersonic wind tunnel was built to facilitate the continued development of **l**ocalized **a**rc **f**ilament **p**lasma **a**ctuators (LAFPAs) as a control method for supersonic mixed compression inlets. A variable angle wedge was employed as the compression surface to generate a variable strength **s**hock **w**ave **b**oundary **l**ayer **i**nteraction (SWBLI). The resulting flow is Mach 2.33 with a Reynolds number based on boundary layer momentum thickness of 23,000. Several qualitative techniques were used to observe certain aspects of the flow and interaction. Schlieren imaging was used during the troubleshooting phase to identify extraneous shock waves and expansion waves and revealed an unwanted separation region on the ceiling. Oil flow visualization on the interaction surface highlights the three-dimensionality of the separation region, but also confirms a two-dimensional assumption near the centerline of the tunnel. The separation region was found to extend 20 mm in the streamwise direction. Particle image velocimetry (PIV) was used to gather quantitative flow field information about the freestream and boundary layer. The incoming boundary layer, measuring 4.62 mm in thickness, will be analyzed in further detail.

ACKNOWLEDGEMENTS

I would like to thank Professor Mo Samimy for his support throughout this research. He was always available for discussion regarding experiments and academics. I would also like to thank my colleagues Nathan Webb and Dr. Edgar Caraballo, who worked closely with me in this project. I am also thankful for the assistance provided by Dr. Jin-Hwa Kim with the surface oil flow visualization technique. In addition, Dr. Jesse Little, Martin Kearney-Fischer, Aniruddha Sinha, Michael Crawley, and Casey Hahn provided productive discussion for which I am grateful.

The support of this research by the Air Force Research Laboratory (Mr. Jon Tinapple and Dr. Jonathan Poggie) and the Air Force Office of Scientific Research (Dr. John Schmisseur) is acknowledged, and greatly appreciated.

TABLE OF CONTENTS

LIST OF TABLES

LIST OF FIGURES

CHAPTER 1: INTRODUCTION

The interaction between an oblique shock wave and a turbulent boundary layer occurs in every supersonic mixed-compression inlet. This **s**hock **w**ave **b**oundary **l**ayer **i**nteraction (SWBLI) generates an adverse pressure gradient that can cause the boundary layer to separate. Boundary layer separation in the inlet reduces the overall performance of the engine due to a decrease in efficiency, increased unsteadiness of the flow, and additional noise. Efforts made to remove the adverse effects of the shock wave boundary layer interaction have become a key point of design in modern jet engines for supersonic aircraft.

The conventional method for preventing separation of the boundary is boundary layer bleed. Bleeding the low momentum fluid near the wall upstream of the interaction region weakens the SWBLI, thereby removing the possibility of separation, but incurs a significant reduction in mass flow. This results in a thrust penalty. To counter this mass flow loss, larger inlets must be used to capture more flow, which results in greater weight and drag.

To avoid this mass flow loss, thereby reducing the overall size and weight of the inlet, recent research has looked into alternatives to the bleed method. Anderson *et al.*[1] investigated the effectiveness of micro-vane and micro-ramp arrays. Micro-vanes and micro-ramps introduce counter-rotating longitudinal vortices in the near wall region that serve to enhance mixing between the high momentum freestream and the low momentum

boundary layer. This energizes the boundary layer thus making it more resistant to separation. Ogawa and Babinsky[2] used three-dimensional bumps to reduce the total pressure loss of a normal-shock wave boundary layer interaction by as much as 30%. Kalra *et al.*[3] used magnetically accelerated surface plasma to control a SWBLI.

Recent development of **l**ocalized **a**rc **f**ilament **p**lasma **a**ctuators (LAFPAs) is a promising solution to shock wave boundary layer interaction control. The actuators generate an arc filament across two electrodes when powered by a sufficiently high voltage. The resultant electrical arc causes rapid localized heating that generates thermal and pressure perturbations in the flow. Rapid pulsing of the actuators at frequencies associated with the instabilities present in the flow can excite these flow instabilities. LAFPAs have previously been used to enhance jet mixing and mitigate jet noise in subsonic and supersonic jets.[4-6]

The use of LAFPAs for SWBLI control has been investigated by Caraballo *et al*.[7] When operated at a characteristic Strouhal number of 0.03, the plasma actuators were observed to energize the fluid in the boundary layer thus effectively controlling the SWBLI.

CHAPTER 2: BACKGROUND

2.1 SWBLI Physics

The interaction between an oblique shock wave and a boundary layer is complex and exhibits many unsteady behaviors. Although SWBLIs have been investigated for over 50 years, the exact mechanisms responsible are still not well understood.[8] In contrast, the structure of SWBLIs has been well characterized. A diagram of a typical SWBLI is shown in Figure 1.

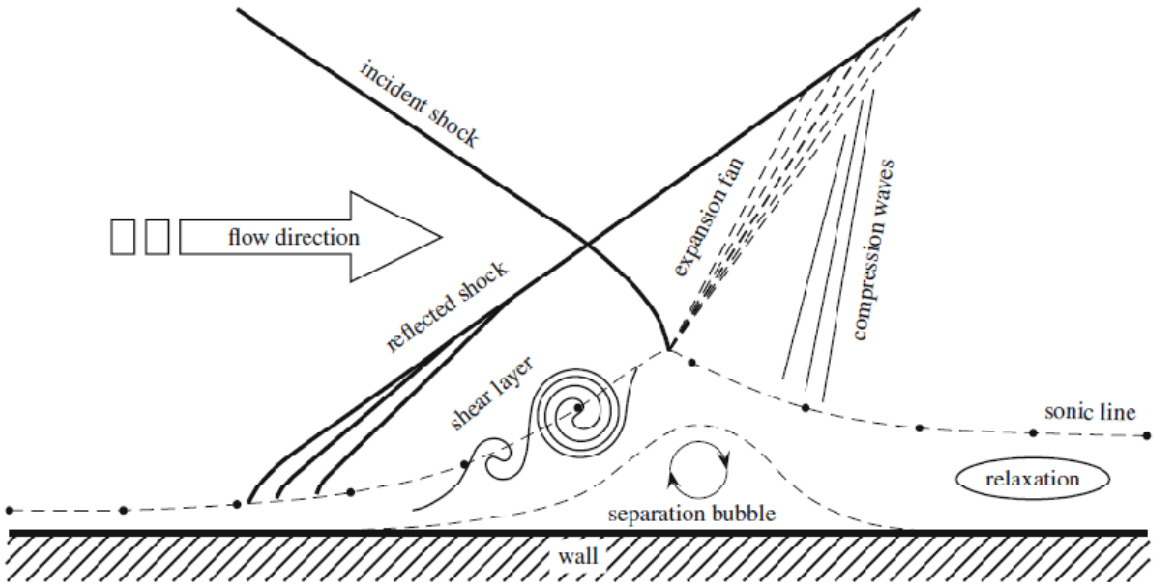

Figure 1. Typical SWBLI[9]

Supersonic flow approaches the oblique shock wave from the left accompanied by some initial boundary layer thickness (δ). As the flow passes through the shock, it is

slowed in the shock-normal direction resulting in a pressure increase. This adverse pressure gradient slows the fluid in the boundary layer, thus thickening it. If the pressure gradient overcomes the dynamic pressure of the boundary layer fluid, the boundary layer will separate. The reverse flow forms a separation bubble, which reduces the effective cross-sectional area of the inlet. This reduces the mass flow rate, causing an overall reduction in performance. The unsteadiness of the separation can destabilize the terminal normal shock, leading to unstart and large unsteady pressure loads, which can damage engine components.

2.2 SWBLI Control Methods

Currently the most common method of preventing SWBLI induced separation is boundary layer bleed. Low momentum fluid near the wall is vacuumed ("bled") from the flow upstream of the interaction. The increase in the momentum of the boundary layer makes it more resistant to the adverse pressure gradient and less likely to separate. Boundary layer bleed is undesirable because it is accompanied by two major losses in performance. Bleeding the flow from the inlet reduces the overall mass capture. To compensate for the reduced mass flow, a larger inlet area is necessary to deliver the proper flow rate. This results in increased weight and inlet drag. Another major loss associated with boundary layer bleed comes from the pressure gradient between the inlet flow and the high-altitude/low-pressure ambient. To remove the high-speed, low-pressure fluid from the inlet, power generated by the engine must be used to create the necessary vacuum. Additionally, the effects of boundary layer bleed are static and do not perform optimally under off-design conditions.[1]

Recent research has investigated alternatives to boundary layer bleed. Anderson *et al.*[1] and Babinsky *et al.*[10] examined the effectiveness of micro-vane and micro-ramp arrays. Micro-vanes and micro-ramps introduce counter-rotating longitudinal vortices in the near wall region, which serve to enhance mixing between the high momentum freestream and the low momentum boundary layer. This increases the overall momentum of the boundary layer and effectively mitigates boundary layer separation. Ogawa and Babinsky[2] used three-dimensional bumps to reduce the total pressure loss of a normal-shock wave boundary layer interaction by as much as 30%. Kalra *et al.*[3] used magnetically accelerated surface plasma to reduce separation. Although low currents (<100 mA) were unsuccessful, higher currents (100-300 mA) were able to delay the incipient separation.

LAFPAs were recently developed at the Gas Dynamics and Turbulence Laboratory for controlling high-speed, high Reynolds number jets for noise mitigation and mixing enhancement.[4-5,11] The control mechanism of the actuators is the excitation of natural instabilities within the flow. LAFPAs offer an active, dynamic solution to SWBLI control without the side effects associated with boundary layer bleed.[7,12] A LAFPA consists of a tungsten electrode pair forming a spark gap. When a sufficiently high voltage is applied, breakdown occurs forming an arc filament. The resultant filament causes rapid localized heating, which generates thermal and pressure perturbations in the flow. These thermal and pressure perturbations can act as a flow control mechanism. An array of LAFPAs operated at the receptive disturbance frequencies present in the flow can be used to excite natural instabilities and effectively control the SWBLI.

2.3 SWBLI Control Using LAFPAs

LAFPAs are an active control technique that can be used to prevent SWBLI induced separation. The LAFPAs have a broad range of operating frequencies: 0-200 kHz. This could allow them to be effective under a wide variety of off-design conditions. In addition, the power consumption of the LAFPAs is fairly low: about 30 W per actuator.[13]

A weighted power spectral density graph of wall pressure under the reflected shock is shown in Figure 2. The figure expresses two peaks, a large broadband peak at St=0.03 and a slightly smaller but much narrower peak at St=0.5. The high frequency energy detected is generated by the turbulence in the upstream boundary layer. The low frequency energy spans at least one frequency decade and is two orders of magnitude smaller than that of boundary layer turbulence. The low frequency content of the reflected shock foot is associated with large-scale low-frequency oscillations of the reflected shock. The exact mechanism that generates these oscillations is still unclear.[9,14]

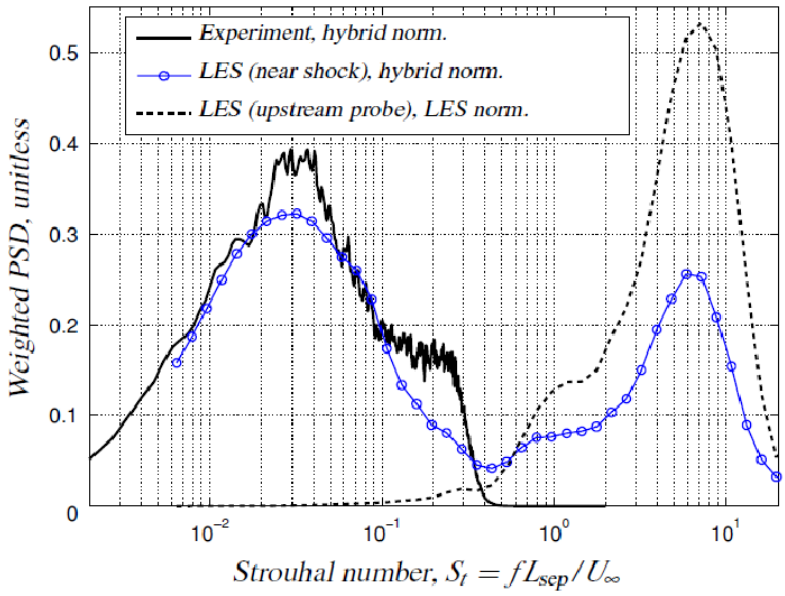

Figure 2. SWBLI frequency content[9]

Several authors believe an upstream influence is responsible for the low-frequency unsteadiness of the shock foot. Beresh *et al.*[15] and Ganapathisubramani *et al.*[16-17] have detected superstructures in the boundary layer. The term *superstructure* refers to a region of high- or low-speed flow with large streamwise extent (up to 70δ has been observed). Superstructures have also been observed by Humble *et al.*[18], although not of the same streamwise extent observed by the previously mentioned authors. These structures have sufficient streamwise extent to generate oscillations at the low frequencies observed. In addition, Beresh *et al.* correlated the reflected shock position with the upstream boundary layer velocity. However, these superstructures are of limited spanwise extent. Therefore, it seems unlikely that they are responsible for the largely two-dimensional oscillations of the reflected shock.

Much research has previously attributed the low-frequency unsteadiness to the separation region.[19-24] However, Piponniau *et al*.[25] seem to be the first to propose a concrete downstream mechanism. They suggest that the entrainment, growth, and eventual shedding of large-scale structures by the shear layer results in expansion and contraction of the separation region. The bubble continuously entrains flow and periodically sheds structures. This generates the observed periodic expansion/contraction. This repetitive cycle of expansion and contraction results in a breathing motion of the bubble, as observed by Touber and Sandham.[9,26] Expansion of the bubble pushes the shock foot upstream and contraction of the bubble relaxes the shock foot downstream. Thus, the breathing motion of the bubble causes the reflected shock foot to oscillate in a large scale, two-dimensional manner.

Pirozzoli and Grasso[27] suggest that an acoustic resonance mechanism may be responsible for the large-scale low-frequency unsteadiness in the interaction zone. The authors propose that vortex shedding near the separation point propagates downstream in the mixing layer. The generation of feedback pressure waves due to the interaction at the foot of the impinging shock propagate upstream as acoustic disturbances. However, the authors were not able to suggest an exact mechanism.

Use of LAFPAs by the Gas Dynamics and Turbulence Lab has shown promising results. A cross-stream flow field (acquired using stereoscopic PIV, discussed in Section 4.3) located just behind a spanwise array of eight plasma actuators is shown in Figure 3. Forcing the actuators at a Strouhal frequency of 0.03 greatly increases the momentum of the boundary layer, thus increasing its resistance against the adverse pressure gradient of the interaction region. Forcing with a Strouhal frequency of 0.5 results in almost no alteration of the boundary layer, however, demonstrating the frequency dependence of the LAFPA control authority over the interaction.

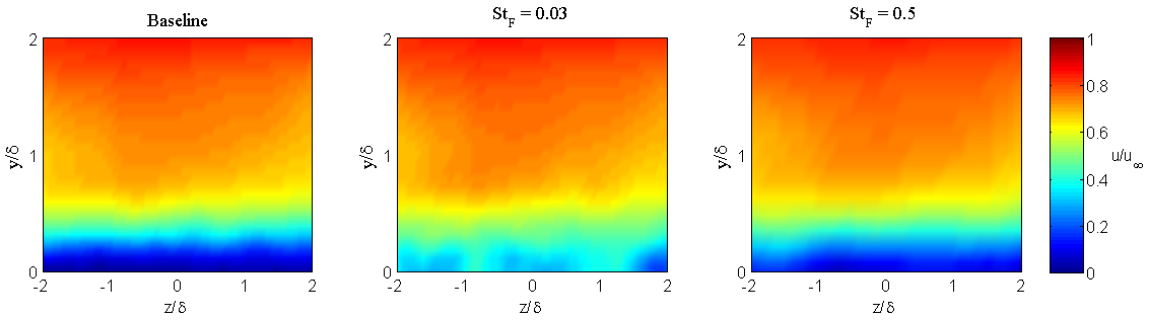

Figure 3. Previous LAFPA effects on boundary layer[7]

The plasma actuators were simulated using thermally-induced surface perturbations by Yan and Gaitonde.[28] The joule heating of near wall flow generated a

pressure bubble resulting in streamwise vortices. This effect is similar to that of mechanical tabs in a laminar boundary layer. Experimental results, however, show no evidence that streamwise vortices are the mechanism responsible for SWBLI control in a turbulent boundary layer. This seems to indicate that instability excitation is the sole control mechanism by which LAFPAs assert control authority in a SWBLI.

2.4 Previous Supersonic Wind Tunnel Facility

In previous work, a Mach 1.89 blowdown wind tunnel was used for testing. The previous wind tunnel test section had a 3.0 inch width by 1.5 inch height. A 10° ramp, positioned on the ceiling, generates a shock wave that interacts with the boundary layer on the floor. The incident shock generated by the compression ramp is inherently unsteady due to the influence of the incoming boundary layer on the ceiling. This additional unsteadiness introduced by boundary layer turbulence increases the overall interaction unsteadiness.

Geometry of the compression ramp facility is fixed. Since shock angle is a function of compression angle and Mach number only, the shock angle is effectively fixed. Only a new supersonic nozzle, with a different design Mach number, or a new ramp, with a different compression angle, would allow for different shock angles. Thus the interaction strength, which is dictated by shock strength (correlated to shock angle), is therefore also effectively fixed, alterable only with new components for the facility.

The geometry of the compression ramp tunnel imposes some limitations on data acquisition. A schlieren image of a typical flow present in the compression ramp facility is shown in Figure 4. The light and dark regions of the image are representative of compression and expansion of the flow. The schlieren imaging technique will be

explained in further detail in Section 4.2 Schlieren Imaging. An expansion fan forms just behind the incident shock at the end of the compression ramp. The expansion fan impinges on the boundary layer followed by several reflected shocks. The interaction between the downstream boundary layer and the expansion/compression waves prevents useful data on the recovering boundary layer from being gathered.

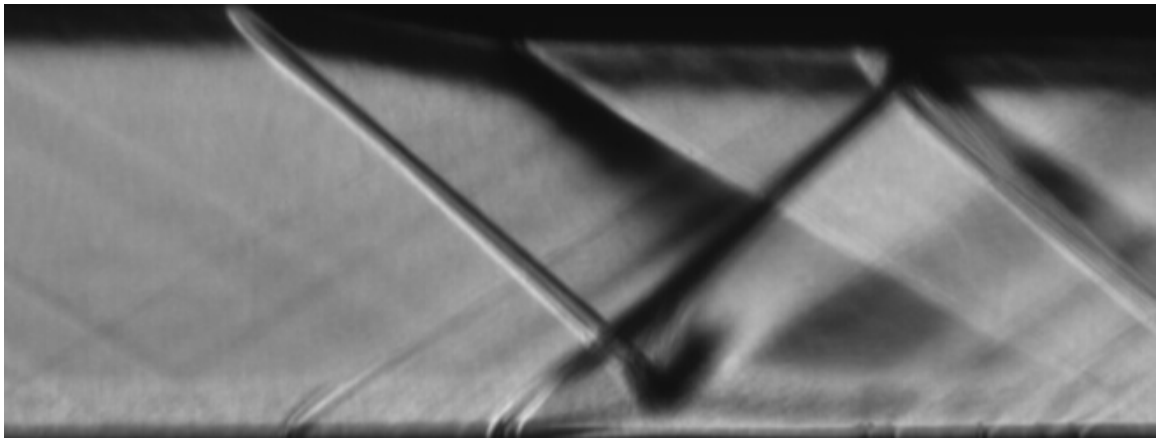

Figure 4. Compression ramp facility

CHAPTER 3: OBJECTIVE

3.1 Further Investigation of LAFPAs

The ultimate goal of this research is to investigate the control authority of LAFPAs on a SWBLI. Many variables contribute to the control authority of the plasma actuators. The variables of most concern are: forcing frequency, streamwise location, spanwise spacing, duty cycle, and mode of operation. Previous research has included frequency, streamwise location, and a limited study of mode of operation.[7,12] Investigation of the effects of these parameters on the LAFPA's control authority should be continued to refine the LAFPA characterization. The remaining variables (spanwise spacing and duty cycle) need to be investigated in detail. It is also of interest to relate the control authority of the plasma actuators to the interaction strength. A stronger interaction, with a larger adverse pressure gradient, is likely to be more difficult to control.

3.2 New Tunnel

To enable further investigation of the LAFPA's control authority over a SWBLI, a new wind tunnel facility is required. The existing facility has yielded high quality data, but does not readily allow for further investigation in some regards. For instance, the interaction strength can be varied only by replacing components of the wind tunnel. Additionally, the recovering boundary layer is distorted due to the impingement of an

expansion fan, which does not allow the possibility of collecting useful data in that region.

According to previous research, for a given Mach number, flow separation is largely affected by incident shock angle.[17,25] Therefore, control over the strength of the shock generated by the compression surface is desired to induce separation in the flow. The use of a compression wedge, instead of a simple ramp, allows adjustability of the compression surface angle and therefore the incident shock strength. The use of a detached wedge will also eliminate shock unsteadiness introduced by the ceiling boundary layer.

It is also desirable to increase the height of the test section. To allow room for the placement of a wedge within the tunnel a larger test section height is required. Additionally, increasing the tunnel height will delay the impingement of the expansion fan generated by the compression surface. The schlieren image shown in Figure 4 shows an expansion fan impinging upon the boundary layer not far from the interaction region; this corrupts the boundary layer preventing the downstream region from providing any useful data. Additionally, a physically larger cross-section has the added benefit of a larger investigation area.

A Mach number between 2.0 and 2.1 is desirable for comparison with available literature and use in the industry. However, it became necessary to increase the Mach number slightly to eliminate undesirable flow conditions. The resultant freestream Mach number is 2.33 based on the absolute static to stagnation pressure ratio. Research done by Dr. Dussauge's group[24] at IUSTI is in a Mach 2.3 flow with an 8° compression wedge, so results gathered will be directly comparable to theirs.

3.3 Validation and Characterization

After the new tunnel's construction is completed, the tunnel will need to be characterized. It must be confirmed that the facility operates properly and as expected. Therefore, it is necessary to validate the resulting flow conditions. Removing extraneous shocks and ensuring the formation of a standard SWBLI are of great importance. In addition, comprehensive baseline flow data will need to be collected for future comparison. A detailed study of the baseline (unforced) flow fields will be performed. Validation and characterization methodology will be discussed in Sections 4.2 through 4.4.

CHAPTER 4: EXPERIMENTAL DESIGN

4.1 Tunnel Design

There are two large observation windows on either side of the tunnel. Each window is made from optical quality fused quartz and measures nominally 3 inches tall, 10 inches wide, and 0.75 inches thick.

Two supersonic convergent-divergent nozzles were designed for the facility using the method of characteristics. For the first iteration of the **v**ariable **a**ngle **w**edge (VAW) facility, a nominally Mach 2.1 nozzle was designed. A FORTRAN program and the Method of Characteristics were used to generate the surface curvature of the rectangular nozzle. A nominal Mach number of 2.1, tunnel height of 2.87 inches, and a throat curvature of 0.25 in^{-1} were used as the relevant parameters. A second nozzle was later designed for a nominal Mach number of 2.57 and a throat curvature of 2.0 in^{-1}.

To control shock strength, a variable angle wedge was attached to the ceiling of the tunnel within the test section. The wedge has four junction points on its upper surface that were attached to thin posts via small pins. Two posts in the front attach directly to the tunnel ceiling. The rear set of posts pass through sealed holes in the ceiling and attach to a linear actuator. A detailed view of the wedge can be seen in Figure 5.

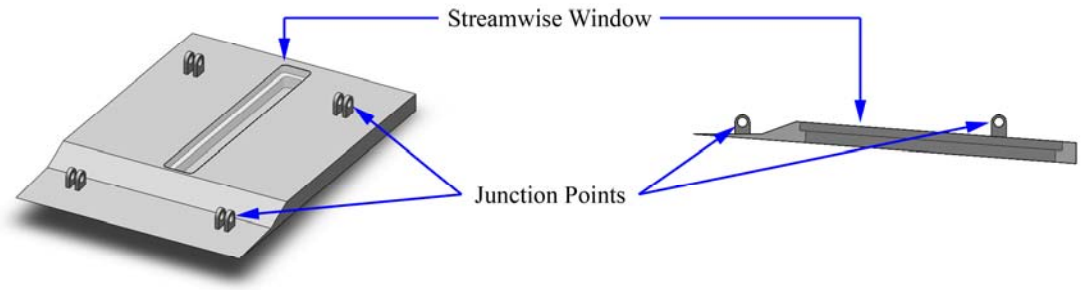

Figure 5. Wedge design detail

The angle of the wedge is controlled by a simple kinematic linkage driven by a linear actuator. The linkage can be seen in Figure 6. A LabVIEW program controls the angle of the wedge. A geometric relation converts the desired wedge angle (in degrees) into the required position of the linear actuator (in steps).

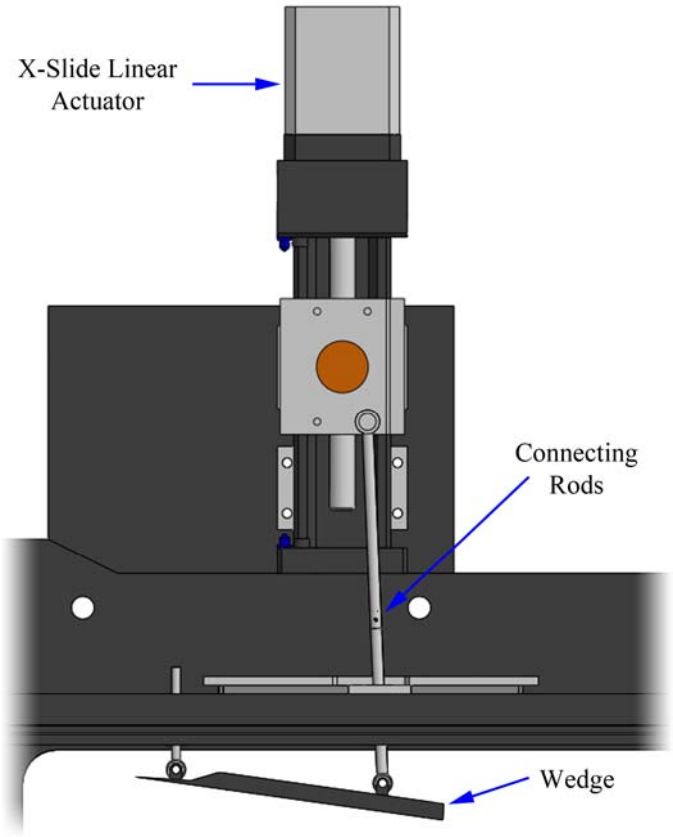

Figure 6. Wedge angle control mechanism

Special care went into the design of the tunnel floor of the test section. A Delrin housing, which acts as the floor, contains a large slot that spans most of the tunnel's width positioned off-center in the streamwise direction. Placed within that slot is a two-piece cartridge, which contains the LAFPAs, also positioned off-center. The eccentricity gives each piece two possible positions, resulting in four possible placements of the plasma actuators along the test section floor. Future actuator cartridges, which would also be designed with an eccentricity, will similarly have four possible placements, allowing a great deal of flexibility for plasma actuator positioning. The test section floor and actuator cartridge can be seen in Figure 7 and Figure 8, respectively.

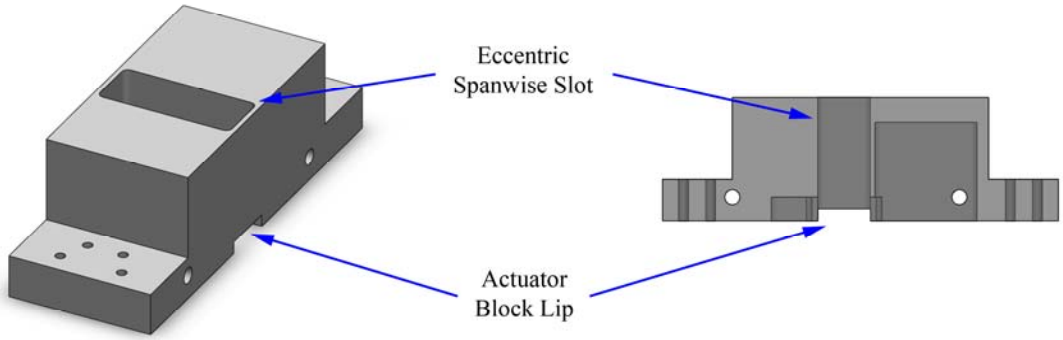

Figure 7. Test section floor

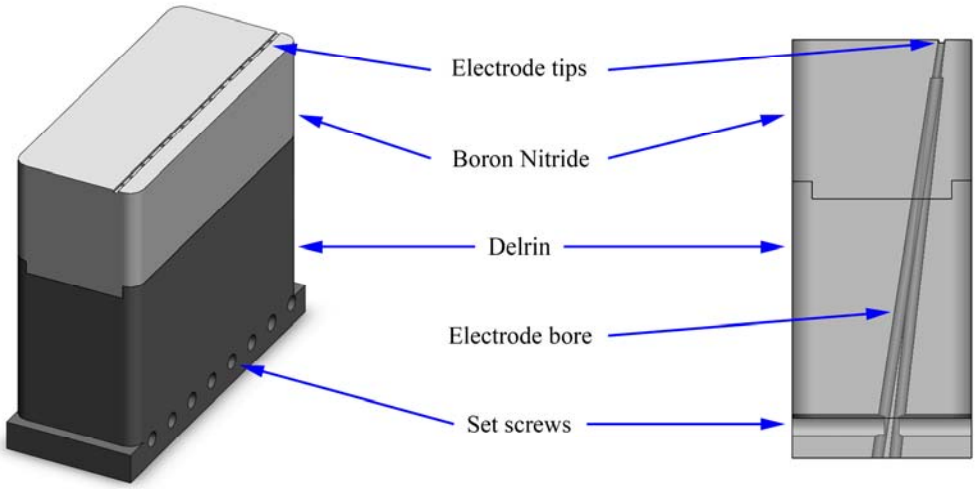

Figure 8. Plasma actuator cartridge

4.2 Schlieren Imaging

The schlieren imaging technique can be used to qualitatively visualize flow phenomenon such as shock waves and expansion waves. Density gradients present in the flow are expressed as light and dark regions in the image. Disturbances in the flow are accompanied by localized changes in density. The Gladstone-Dale relation connects these changes in density by a proportional change in refractivity.[29] A collimated beam of light

shining across the flow is focused with a mirror to a knife-edge at the focal point before entering a camera.The collimated light experiences small deflections as it passes through the flow due to the differences in refractivity. This causes portions of the light to be blocked by the knife edge before entering the camera.The result is light and dark portions of the image corresponding to positive and negative fluid density gradients in the direction normal to the knife-edge. The optical components used to gather schlieren images are detailed in Table 1 and arranged as in Figure 9. This configuration results in a spatial resolution of 6.4 pixels/mm.

Table 1. Schlieren optical specifications

Component	Specification
Camera	Sony XCD-SX910 (1376x1024 pixels)
Focal lens	Nikon Micro-Nikkor-P Auto, 1:3.5, f = 55 mm
Filter lenses (2x)	Hoya 52 mm PL
Light source	PalFlash 502 High intensity illumination Flash
Mirrors (2x)	Parabolic, 8 inch diameter, f = 6 ft.
Software	NI LabVIEW 8 with NI-IMAQ camera control

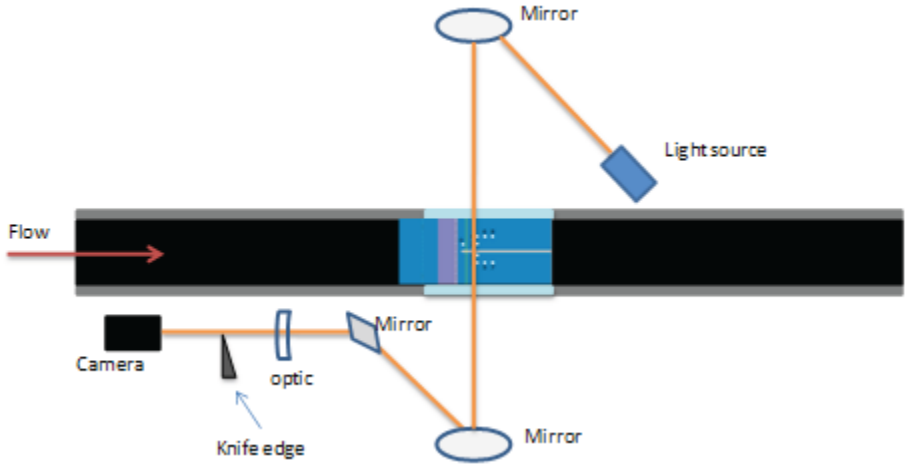

Figure 9. Optical configuration for schlieren imaging

A key use of schlieren imaging is to verify flow quality. The flow will be checked for extraneous shocks and expansion waves to maximize flow cleanliness. The incident shock will be characterized by its angle of incidence, relative strength, and impingement point. These values will be used to choose an appropriate compression wedge angle and subsequent plasma actuator placement.

The schlieren imaging results will also be used to identify optimal placement of the plasma actuators and normalizing parameters such as interaction length. Once the appropriate flow conditions have been determined, the nominal impingement point of the incident shock wave can be identified. Using the impingement point as a reference, the LAFPAs can be positioned accordingly. The size and strength of the interaction region will also be observed.

4.3 Stereoscopic PIV

Stereoscopic **p**article **i**mage **v**elocimetry (PIV) will be used to gather quantitative flow field information. Small tracer particles are injected into the fluid upstream using a TSI 6 Jet atomizer and assumed to track the flow accurately. A laser sheet oriented in the plane of interest is pulsed twice in rapid succession, about 1μs apart, light scattered by the particles passing through the sheet. Two cameras capture an image of the scattered light with each pulse. Every two pulses of the laser sheet generate an image pair for each of the two cameras. A computer can generate a two-dimensional velocity field from each image pair by tracking the displacement of particles over the pulse separation time. Simultaneous velocity fields corresponding to each camera can then be combined into a single three-dimensional flow field using an image correction function. The optical

components used to gather PIV images are detailed in Table 2 and arranged as in Figure 10. This configuration results in spatial resolutions around 24 pixels/mm, depending on camera placement.

Table 2. PIV optical specifications

Component	Specification
Cameras (2x)	LaVision Imager Pro CCD (2048x2048 pixels)
Focal lenses	Tamron SP, 1:2.5, f = 90 mm
Filter lenses	532 nm bandpass filter
Laser	Spectra Physics PIV 400 Nd:YAG, 532 nm wavelength
Cylindrical lens	Convex, f = 15 mm
Spherical lens	Convex, f = 100 mm

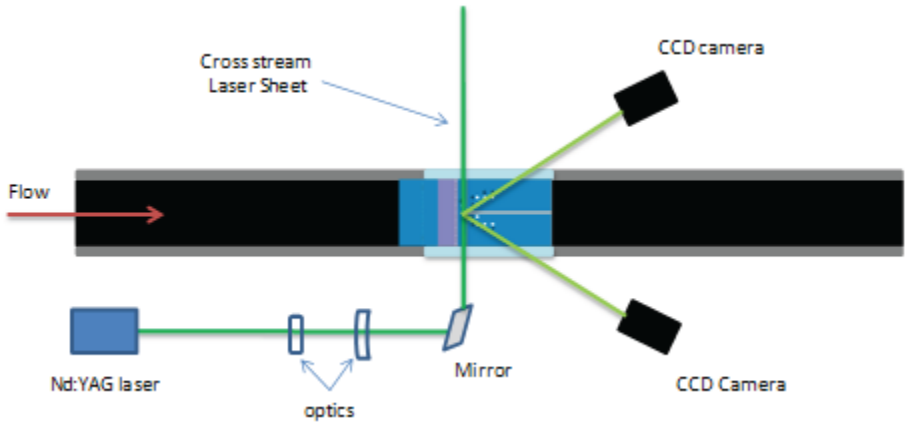

Figure 10. Optical configuration for stereoscopic PIV

The goal of the PIV investigation is to characterize the flow fields at a number of cross-stream planes. An upstream plane will provide incoming flow conditions, particularly the incoming boundary layer profile. A downstream plane will verify the recovery of the boundary layer. A number of planes beginning just upstream of the actuators and ending just downstream of the interaction will be investigated to observe the development of the interaction, especially under actuator forcing conditions. In

addition to the baseline case, active forcing cases will also be gathered for several planes. Flow fields with actuator forcing at Strouhal numbers of 0.03 and 0.5 will be gathered at each plane as well as some less receptive frequencies (e.g. 0.06), except for the far upstream and far downstream planes where the effects of forcing are negligible. The resultant data will be used to assess the effectiveness of the actuators. Comparison of each forced case with the baseline can expose the forcing effect on the flow field.

4.4 Surface Oil Flow Visualization

To gain more qualitative information about the interaction region, surface oil flow visualization will be performed on the interaction surface. PIV and schlieren imaging have difficulty resolving all the way to the surface, making it difficult to gain information about a separation region, which may be less than a millimeter in height; PIV presented in this thesis resolved down to about half a millimeter from the surface. Surface oil flow visualization, however, smears oil on the surface by shear stress, thus highlighting streamlines of the flow. This allows the researcher to characterize a separation region's length, width, and overall shape.

A thin layer of oil is spread uniformly over the surface of interest. In the case of this thesis, a mixture of Titanium-White acrylic paint and SAE 85W-140 gear oil in roughly equal volumes left to cure for several hours before use provided the best results. The oil mixture is then spread thinly onto the removable test section floor by hand using latex gloves. The floor is inserted into the test section and the facility is swiftly started to minimize the transient time. While the tunnel is operational, live images of the oil smearing are taken using a digital camera, which are later deskewed using software. The

camera body used is a Nikon D40 with a Nikon AF-S Nikkor 18-55 mm zoom lens. After at least 15 live images are taken (at a rate of about 1 Hz), the tunnel is quickly stopped to minimize distortion of the oil. The test section floor is then removed, so a top down image can be taken. This method was used to determine the length of separation (L_{sep}) – later used as a normalization parameter.

CHAPTER 5: EXPERIMENTAL RESULTS

5.1 Schlieren Imaging Results and Troubleshooting

The first set of schlieren images recorded for the new tunnel is shown in Figure 11 and Figure 12. A pressure bubble, which formed above the wedge at low pressures, caused a shock wave to form at the leading edge of the bubble. The effect of this pressure bubble was to divert flow to the underside of the wedge. Therefore, a greater mass flow was passing under the wedge than was intended.

Schlieren imaging has the inherent effect of spatially averaging the density gradients in the spanwise direction for this configuration. As such, some of the flow features appear blurred or out of focus. This blurriness is due to the partial three-dimensionality of the flow. While nominally two dimensional about the centerline, the flow is three-dimensional in the near wall region, as determined from later surface oil flow visualization data. The presence of boundary layers on the sidewalls acts to distort the shocks and expansions near the wall, which has a small effect on the spanwise average. It will be shown in Section 5.3 Surface Oil Flow Visualization that there are SWBLIs present on the tunnel sidewalls. In addition, white streaks below the wedge are thought to be caused by high-pressure air from above the wedge bleeding around the edges, since the wedge does not form a seal with the windows.

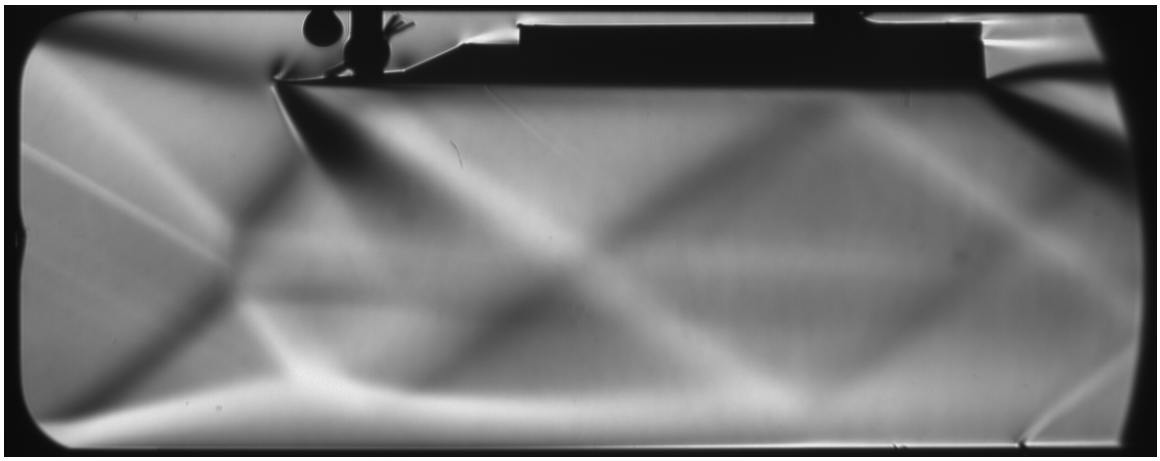

Figure 11. Initial schlieren image of VAW facility

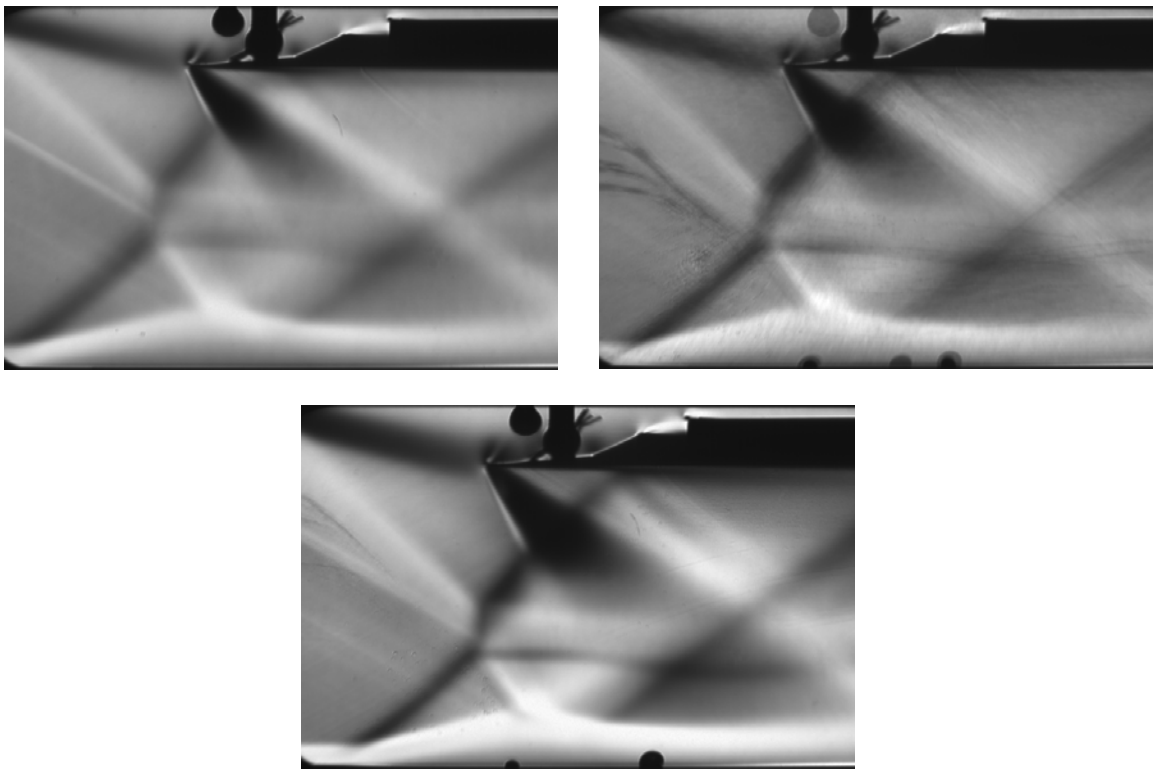

Figure 12. Initial schlieren images of VAW facility

a) p_0= 21 psig; b) p_0 = 30 psig; c) p_0 = 42 psig

The effect of the stagnation pressure on the pressure bubble shock wave could be observed by gradually increasing the stagnation pressure. As the stagnation pressure increased, and therefore the static pressure throughout the flow increased, the pressure bubble above the wedge shrunk slightly moving the shock wave further downstream and close to impinging upon the top of the wedge. It was concluded that adjusting the wedge height might allow the pressure bubble to move downstream and remove its effects from the flow.

Lowering the wedge would allow greater flow above the wedge, thus reducing the adverse pressure gradient. However, it would also capture a greater fraction of the mass flow. The wedge was lowered by placing two thin (~1.5 mm thick each) washers between the front posts and the ceiling. The vertical orientation of the linear actuator allowed it to be adjusted easily and then recalibrated at its new zero. In addition, a small U-shaped bracket, designed to hold a window or window-blank in place, was removed from the topside of the wedge; the window-blank was glued in place using RTV for the remainder of the experiments presented here. The results of lowering the wedge are shown in Figure 13.

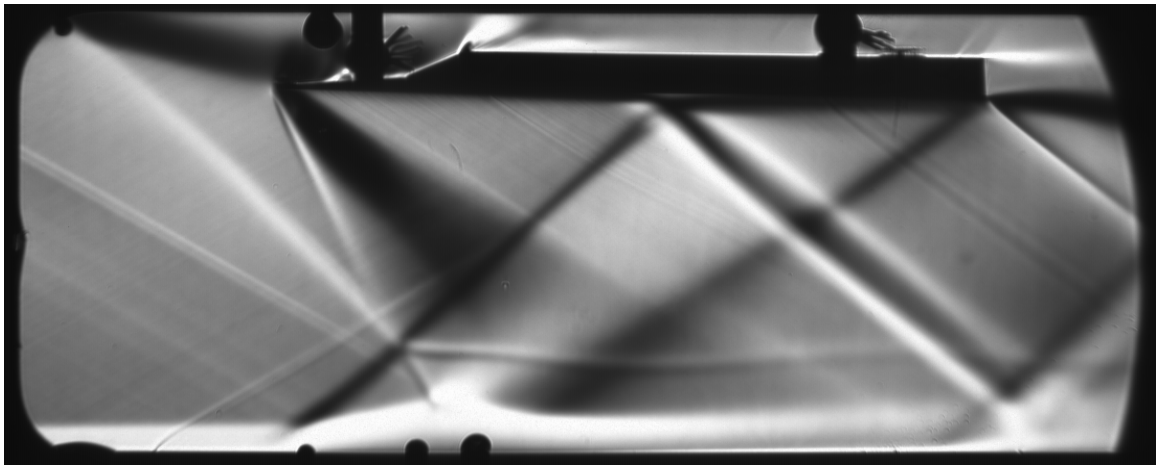

Figure 13. Schlieren with wedge positioned low, p_0 = 30 psig

It can be seen in Figure 13 that lowering the wedge brings the leading edge below the separation on the ceiling. The result is a more recognizable shock forming at the leading edge of the wedge. However, this shock is immediately followed by a large expansion fan and interacts with a shock wave that forms upstream of the ceiling separation.

Raising the wedge would divert less of the mass flow above the wedge. However, the decreased clearance would result in an increased pressure gradient. The wedge was raised by fabricating new, shorter front posts. The results of raising the wedge are shown below in

Figure 14.

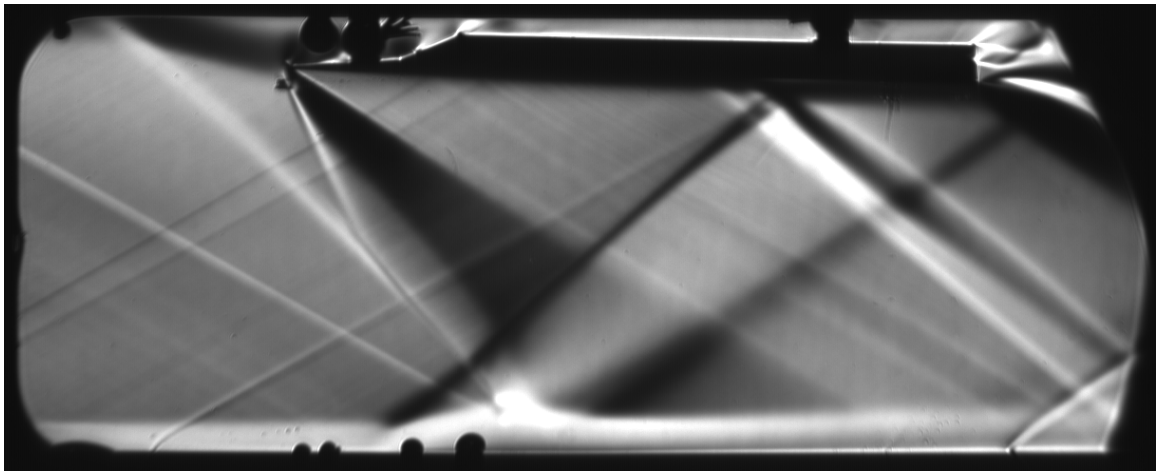

Figure 14. Schlieren with wedge positioned high, p_0 = 21 psig

Raising the wedge had the effect of shrinking the ceiling separation region and moving it downstream. However, the change was not significant enough to solve problem. An oblique shock wave still forms at the leading edge of the separation region, interfering with the incident shock wave of interest. It can also be seen that the separation region interacts with the wedge tip, further corrupting the possibility of a steady incident shock.

Since the state of the flow showed no improvement in the high or low positions, intermediate positions were also tested. A moderate-low position was tested using only one set of washers between the front posts and the ceiling. A moderate-high position was also tested using one set of washers with the short posts. No improvements were observed in either of these two cases. All of the test wedge positions are tabulated below in Table 3, measured from the rotational point of the front posts to the floor surface.

Table 3. Wedge height positions

Position	h/δ	h/L_{sep}
1	9.78	3.04
2	9.47	2.95
3	9.14	2.84
4	8.83	2.75
5	8.51	2.65

Since altering the wedge height has a give and take relationship between mass flow capture and adverse pressure gradient, an alternative method for allowing the pressure bubble to clear was investigated. Mass flow above the wedge was increased by increasing the available flow area. Removing the U-bracket from the topside of the wedge, as mentioned previously, allowed some additional flow area. A trapezoidal section of the ceiling was machined away to create more room for the flow without increasing the capture area. This section was positioned such that the pressure bubble should freely expand into the available volume. The wedge itself was also modified to allow greater flow area. Lengthwise channels or flutes were cut into the topside of the wedge. Modifications to the tunnel are highlighted in Figure 15.

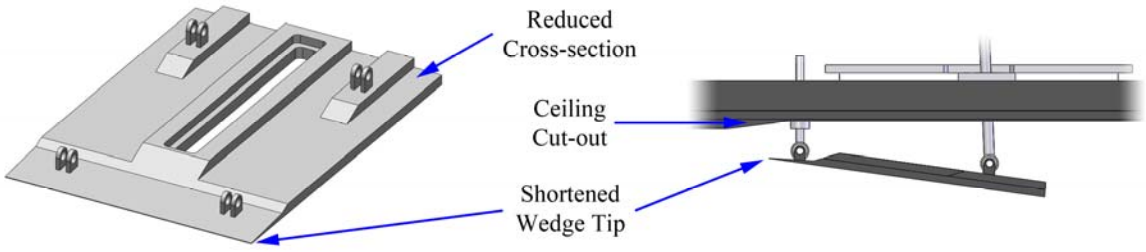

Figure 15.Modified wedge and tunnel ceiling

The results of these alterations are shown in Figure 16. The increased flow area above the wedge displayed a significant improvement in flow quality. The pressure bubble is still present, but has been pushed downstream.

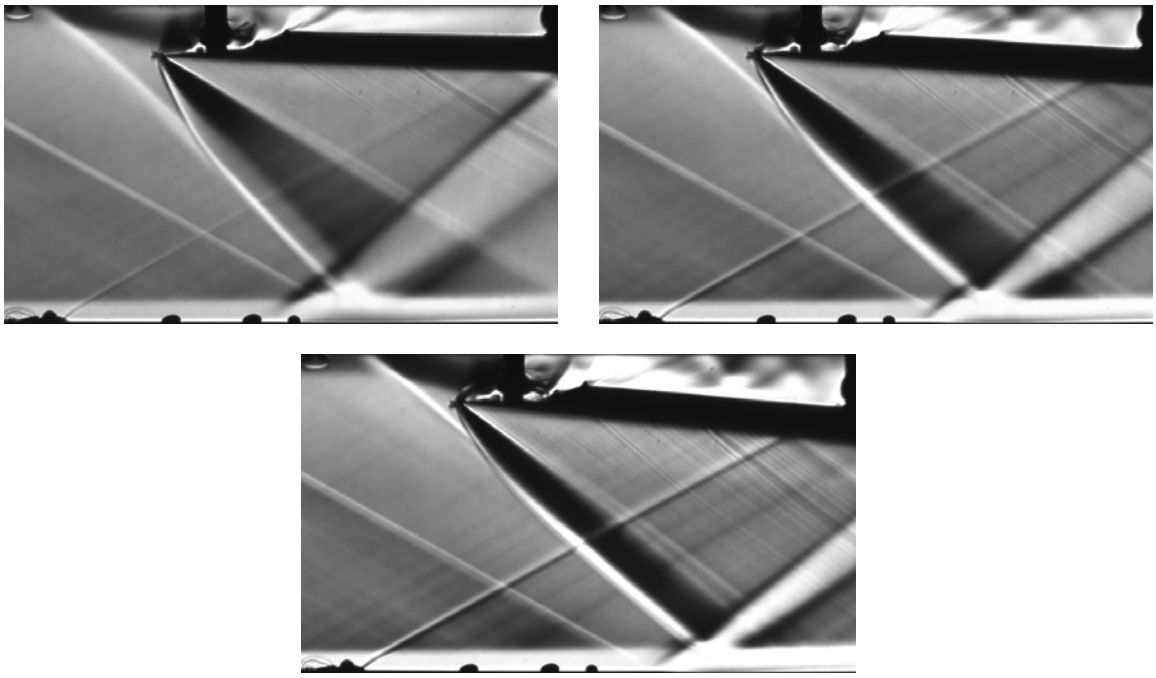

Figure 16. Schlieren with increased flow area over the wedge

a) p_0 = 21 psig, α = 0°; b) p_0 = 30 psig, α = 3°; c) p_0 = 48 psig, α = 5°

Since the pressure bubble that forms above the wedge was believed to have a pressure greater than atmospheric, it should be possible to bleed the high-pressure fluid without a vacuum system. Unplugging an existing slot (intended for a window to allow for a streamwise laser sheet) and existing holes (intended for alternative mounting of the compression wedge) allows for some of the high-pressure fluid above the wedge to escape the tunnel.

Using the above technique resulted in noticeable gains in the schlieren imaging results. However, the gains were not significant enough to produce a sharp incident shock wave as desired. To enhance this effect further, an angled bleed slot was cut out of the ceiling just behind the leading edge of the wedge. The results of this modification are shown in Figure 17. When run at a sufficiently high pressure, the shock originating from the pressure bubble impinges upon the top of the wedge, resulting in a clean incident shock from the compression surface.

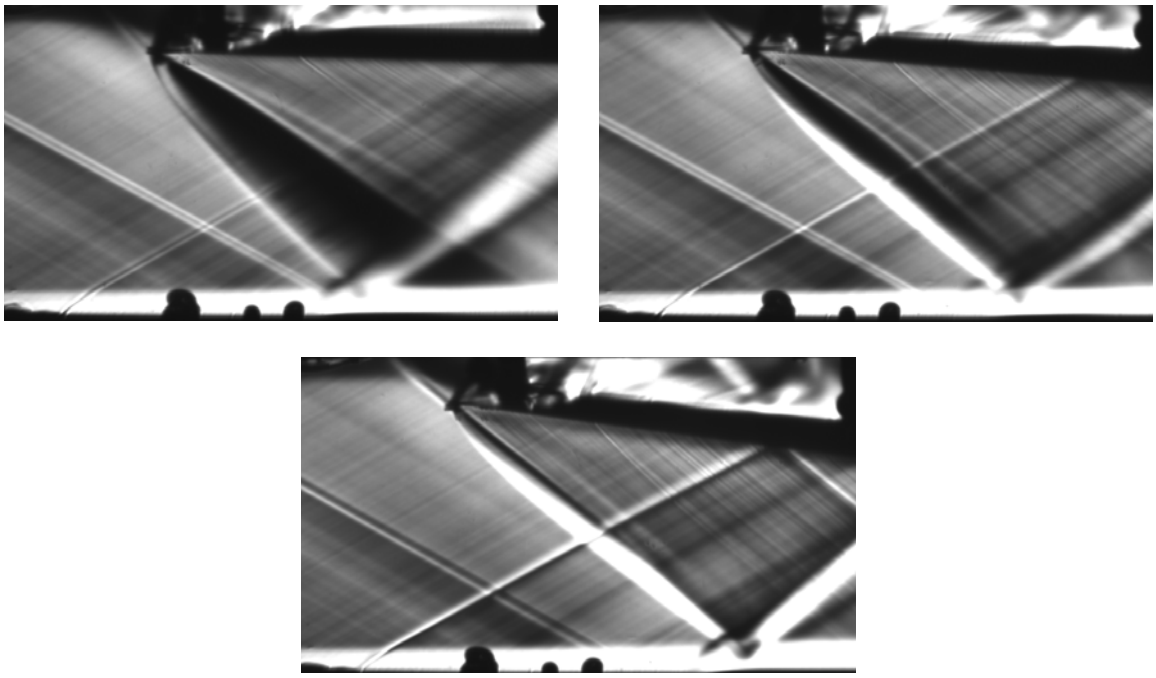

Figure 17. Schlieren with bleed slot above wedge, p_0 = 75 psig

a) α = 0°; b) α = 5°; c) α = 8°

After successfully starting the tunnel with the compression wedge aligned horizontally, the tunnel would become choked and unstart when the wedge angle was increased. This makes sense for significant angles of the wedge, when the area under the wedge becomes aerodynamically smaller than the nozzle throat. However, tunnel unstart

was occurring at small wedge angles, between 5 and 6 degrees. This was unacceptable, since wedge angles between 6 and 9 degrees are required to achieve reasonable shock strength.

It was thought that perhaps the shock-train, which originates at the nozzle and moves downstream during startup, was becoming stuck beneath the wedge. If this were true, then the wedge would be acting as the tunnel diffuser, instead of the diffusion section as intended. As the shock-train moves downstream, it is caught by the secondary choke point—the smallest cross-sectional area beyond the nozzle throat. The critical area of the flow increases in the downstream direction as it passes through the shock waves. It is possible that as the shock-train is moving downstream, the area beneath the wedge is less than the critical area at some location within the shock-train. To ensure that the shock-train was properly captured by the diffusion section, rather than the wedge, the cross-sectional area within the diffuser was reduced. An aluminum extension was designed for the diffuser section of the tunnel. This served to reduce the throat area of the diffuser, ensuring that it was the secondary choke point within the tunnel.

Once this alteration was made, the empty tunnel would start, but failed to do so with the wedge in place. The addition of the extension was reducing the diffuser area too much for the shock-train generated by the wedge, thus causing the flow to choke in the diffuser. The diffuser extension was then reduced and reinstalled, resulting in an effective diffuser somewhere between the original and the first extension. The results of adding the smaller extension (larger cross-sectional area) are shown in Figure 18.

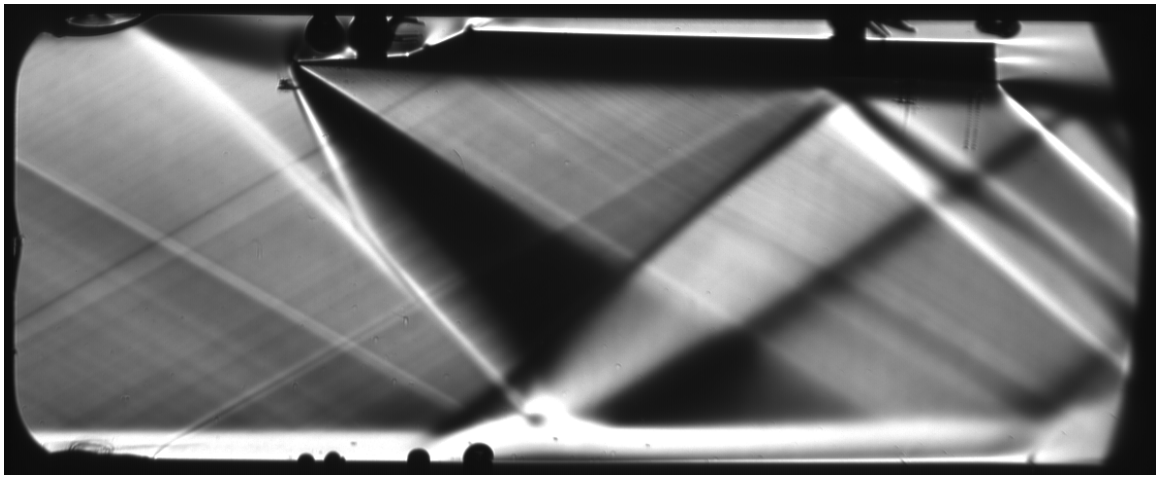

Figure 18. Schlieren with diffusion area slightly reduced

With the modified extension in place, the tunnel started with the wedge, but would unstart when the wedge angle was increased. It was concluded from this experiment that the shocks observed in the schlieren were not the shock-train. If they had been part of the shock-train this experiment would have improved the flow quality, not degraded it.

The next attempt to ensure that the flow was fully supersonic was to lower the pressure in the test section. The downstream diffuser was removed from the tunnel. Eliminating the downstream diffuser allows the shock-train to exit the tunnel, thus forcing the trailing edge of the tunnel to operate closer to atmospheric pressure. The upstream portion of the tunnel will remain below ambient, since the shock-train generated by the wedge acts as a diffuser. By forcing the test section to operate near atmospheric pressure, it guarantees that the nozzle remains at its supersonic design point at the cost of exhausting the high-pressure air tanks more quickly. The result of the modification had only a minor impact on the flow quality.

It was then decided to move on with the data acquisition process and begin gathering PIV data, despite the less than ideal flow conditions. It was discovered that, while operating at high stagnation pressures, even the high-pressure particle seeder borrowed from another project was not able to produce high enough seed particle density to result in high quality PIV data. Therefore, it became necessary to lower the stagnation pressure. The final flow conditions are illustrated below in Figure 19. The investigative cross-stream planes used during the PIV process are illustrated in Figure 20and tabulated in Table 4.

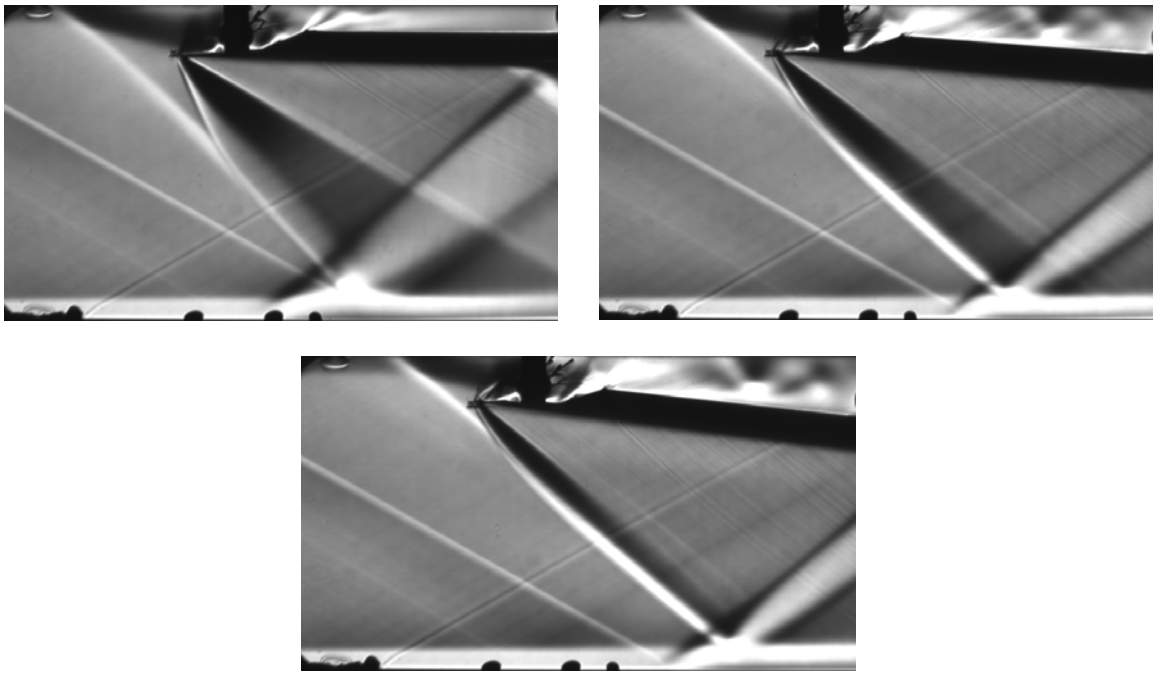

Figure 19. Schlieren for M2.05 PIV, p_0 = 30 psig

a) α = 0°, b) α = 5°, c) α = 7°

The SWBLI location as determined from the schlieren images was used to position the LAFPAs and the investigative planes. The appropriate placement of the

LAFPAs was decided based upon the nominal impingement point of the incident shock wave. The ideal location of the actuators is just upstream of the reflected shock foot, which is thought to be the critical point of the reflected shock instability, and therefore most responsive to control. The five planes of interest described in Chapter 3 were chosen based on the location of the actuators and the lambda-shock structure. The cross-stream planes of interest are shown in Figure 20 and detailed in Table 4. These planes include: far upstream (1), for incoming boundary layer data; just upstream of the actuators (2), for a 'before' image; just downstream of the actuators (3), for an 'after' image; within the separation region (4), to observe the interaction; and, far downstream (5), to verify boundary layer recovery. The results of this PIV investigation were not conclusive and highlighted the need for a cleaner flow; therefore, they will not be discussed in this thesis.

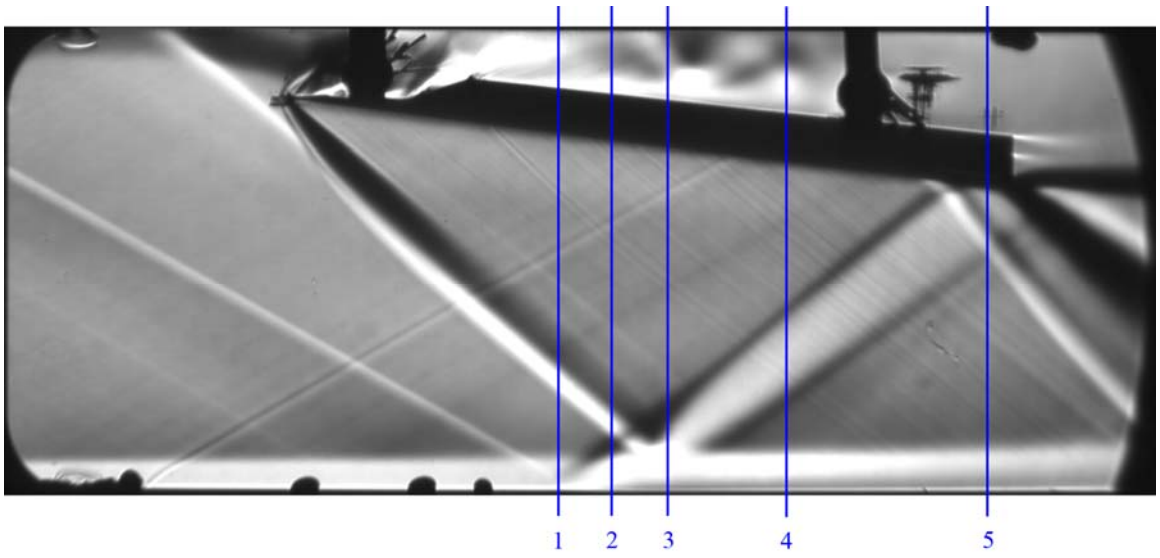

Figure 20. Investigative planes for M2.05 PIV

Table 4. Investigative planes for M2.05 PIV

Plane	x/δ	x/L_{sep}
1	-3.30	-1.03
2	-2.01	-0.63
3	-0.57	-0.18
4	2.33	0.72
5	7.96	2.47

A sharper shock structure was still desired. Moving to a higher Mach number would increase the shock strength and should push the ceiling separation bubble downstream. A new convergent-divergent nozzle was designed using a program that utilizes the method of characteristics. The results of the higher Mach number flow are shown in Figure 21. The operational Mach number of the new nozzle was determined to be 2.33 based on the static/stagnation pressure ratio.

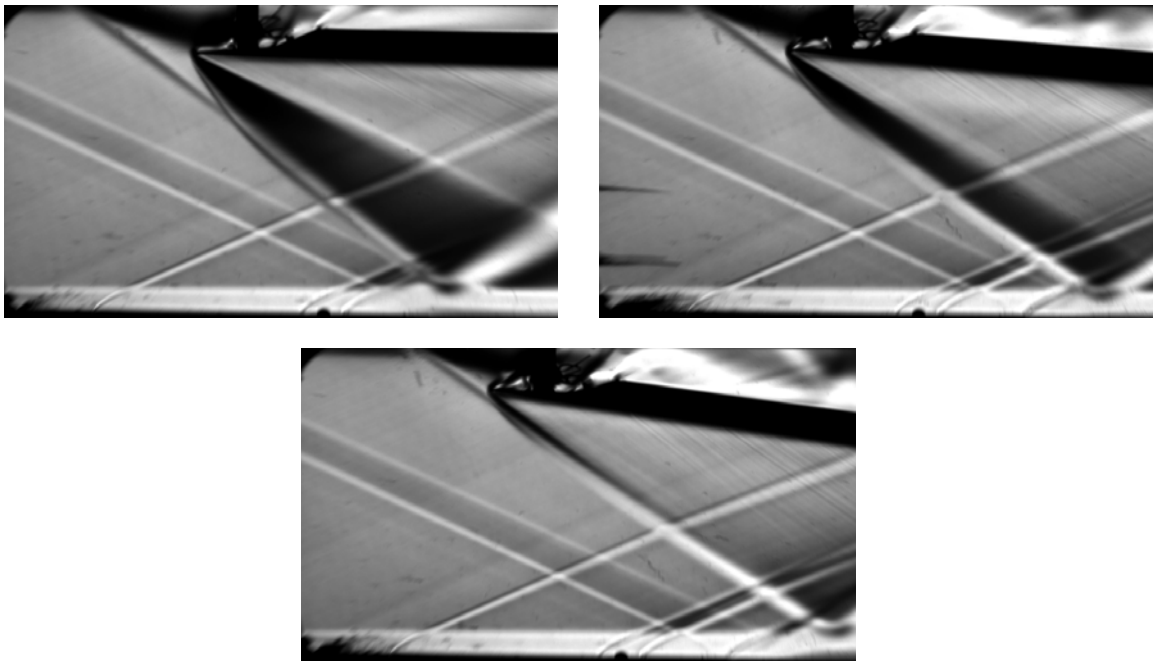

Figure 21. Schlieren for M2.33 PIV, p_0 = 48 psig

a) α = 0°, b) α = 5°,c) α = 8°

The increase in Mach number yielded definite improvements. It can be observed that the shock originating from the pressure bubble is still coalescing with the shock attached to the compression wedge. The nature of the coalescence resembles a bow shock at low wedge angles, but is dominated by the attached shock at higher angles resulting in a sharp shock structure. The Mach 2.33 configuration with a stagnation pressure of 48 psig and a wedge angle of 8° was used for additional PIV. The investigative planes used for the Mach 2.33 PIV are shown in Figure 22 and detailed in Table 5.

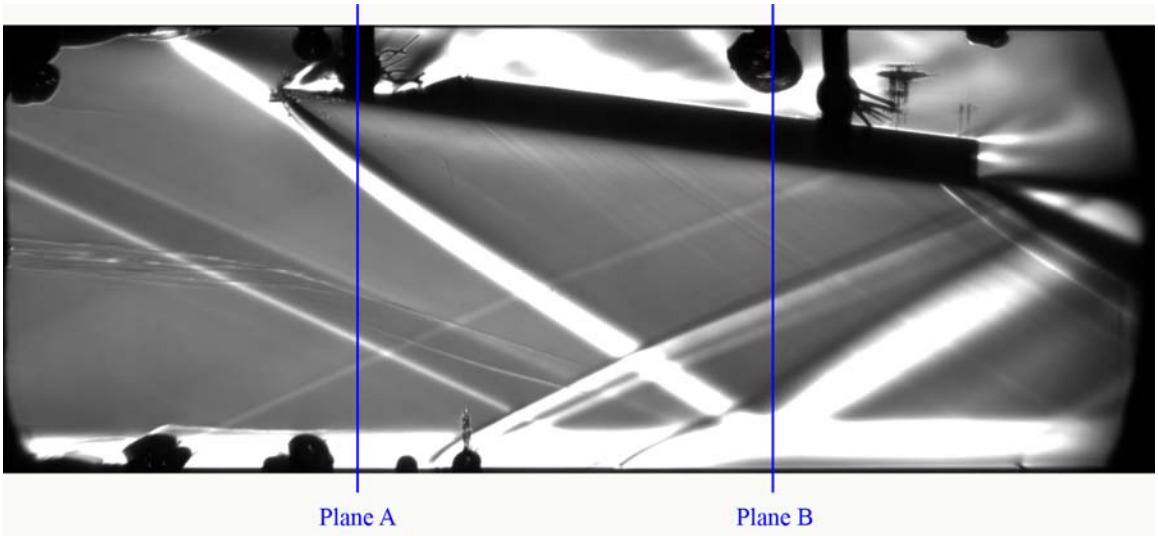

Figure 22. Investigative planes for M2.33 PIV

Table 5.Investigative planes for M2.33 PIV

Plane	x/δ	x/L_{sep}
A	-11.7	-3.63
B	-1.22	-0.38

5.2 Stereoscopic PIV Results

Although flow conditions were not ideal while operating at Mach 2.05, it was thought that the data might yield some useful insights. First attempts at gathering PIV

data at the high pressures desired for relatively clean flow resulted in poor quality data. The pressure seemed too high for the oil particle seeder to produce sufficient particle density (~6 particles per interrogation window). A high-pressure seeder was borrowed from another experiment at GDTL to inject a greater number of particles into the stagnation chamber. The equipment change did increase the particle density, however, it was not sufficient, so additional means were investigated.

Alternative inject ports were investigated to observe their effect on the raw (unprocessed) PIV images. The standard particle injection port used is located in the center of the stagnation chamber. There are several other injection ports available for seeding, two of which were of interest. The first is just upstream of the stagnation chamber, directly into the high-pressure piping that supplies air to the facility. Oil particle injection into this upstream port proved impossible, as the static pressure was higher than the backpressure rating of the seeder. The other injection port of interest is located further downstream, but still within the stagnation chamber. Particle injection closer to the nozzle resulted in a greater seed particle density; however, the seed particle density for this configuration was highly non-uniform.

To gain quality PIV data in a timely fashion, it was decided to operate the tunnel at a stagnation pressure of 21 psig instead of 75 psig. Although this resulted in a lower quality flow, it provided a seed particle density sufficient for PIV processing. To avoid tunnel choking at the newly lowered pressure, the wedge angle was decreased from 7.5º to 7.0º.

When operating the LAFPAs at and above frequencies of 1 kHz, **e**lectro**m**agnetic **i**nterference (EMI) became problematic. The effects of EMI had the most effect on the

laser trigger. A corrupted trigger signal can prevent the laser from successfully firing, resulting in essentially blank PIV images. Due to the nature of EMI, the severity varies from day to day and test to test. However, at its most severe, it can completely incapacitate the laser trigger, making it impossible to record useful data.

Instead of trying to shield the laser trigger to keep its signal pure, it was decided to combat the problem at its source. The high voltage cables, which connect the plasma actuators to the high voltage power supplies, were shielded to prevent the high energy EMI from escaping into the laboratory. Although many temporary solutions were tested, the final solution was to thread the high voltage cables through concentric conducting and insulating tubes. A 1.5-inch diameter steel pipe that shares a common ground with the actuators creates an effective Faraday cage around the high voltage cables. A 1-inch diameter PVC pipe placed concentrically inside the steel pipe maintains roughly equidistant spacing between the cables and the steel piping; this should minimize any capacitive effects of the steel.

Once conditions facilitated quality PIV data, approximately 400 image sets were recorded for each investigative plane. A single image set is comprised of four images, one pair per camera. Each image set was processed using LaVision DaVis 7.2 software. The flow fields for each plane were then ensemble averaged and cropped using Mathworks MATLAB R2007b. The streamwise components of the flow fields are presented below, with a color map representation of the streamwise magnitude. For each PIV figure, the nominal flow direction (+x) is oriented normal to the page toward the reader. An ensemble average of the baseline flow at Plane A is shown in Figure 23.

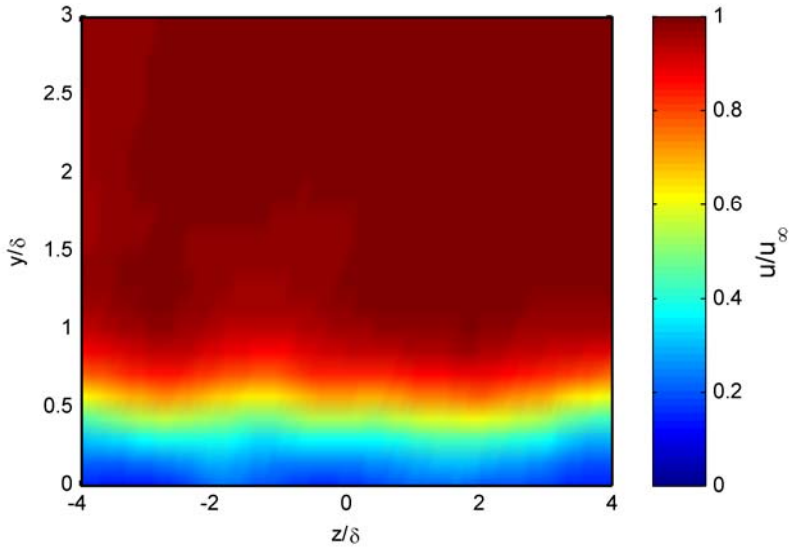

Figure 23. M2.33 baseline flow at plane A

It can be seen from the flow field of Plane A, that the streamwise velocity is approximately two-dimensional within the crop limits. The freestream flow, measuring 542.5 m/s, appears uniform and displays a smooth boundary layer near the wall.

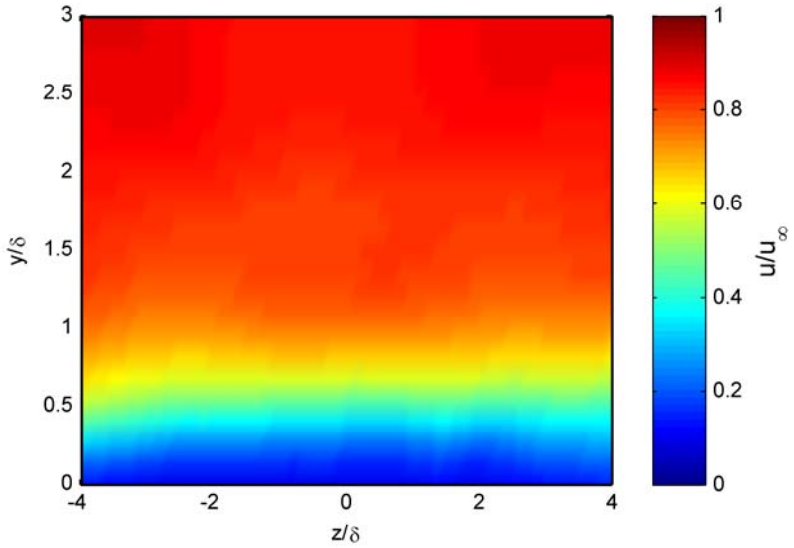

Figure 24. M2.33 baseline flow at plane B

From plane B, it can be observed that the streamwise velocity is uniform and approximately two-dimensional. Note that the freestream flow is approximately 0.9 u/u_∞ at this downstream location.

The flow field at plane A was analyzed further to gain insight of the incoming boundary layer. The streamwise component of the velocity was spanwise averaged to generate the boundary layer profile presented in Figure 25. Note that the error bars represent the RMS velocity in the streamwise direction.

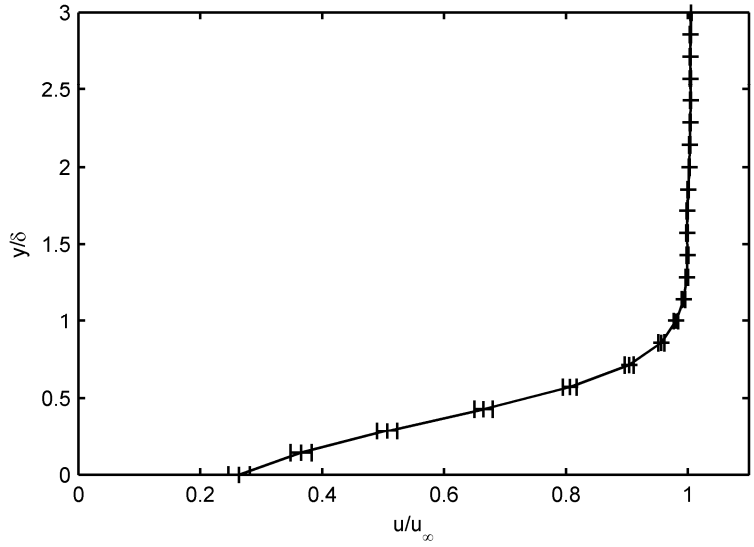

Figure 25. M2.33 boundary layer profile at plane A

The incoming boundary layer appears healthy and full. Several characteristic values were calculated based on the boundary layer profile. The corresponding displacement thickness (δ^*) and momentum thickness (θ) are 2.15 mm and 0.62 mm, respectively. The shape factor (H) is 3.84. Comparison with similar experiments is shown in Table 6.

Table 6. Comparison of characteristic values

Group	M_∞	U_∞ [m/s]	δ [mm]	δ* [mm]	θ [mm]	H	Re_θ
GDTL	2.33	543	4.62	2.15	0.47	3.59	23,000
Dupont *et al.*[23]	2.3	556	11.0	n/a	1.28	n/a	6,900
Piponniau *et al.*[25]	2.28	550	11.0	3.40	0.96	n/a	50,000

Maise and McDonald[30] proposed a normalization technique for turbulent compressible boundary layers using the van Driest transformation. The van Driest transformation is obtained by introducing compressibility into the derivation of law of the wall. The generalized velocity profile is given by

$$\frac{u_\infty^* - u^*}{u_\tau} = -\frac{1}{\kappa}\ln\left(\frac{y}{\delta}\right) + \frac{\Pi}{\kappa}\left(1 + \cos\frac{\pi y}{\delta}\right) \quad \textbf{Eq. 1}$$

where κ=0.4 is the Karmen mixing length constant, Π is an unknown skewness factor, and u_τ is an unknown friction velocity. The normalized velocity, u^*, is given by

$$u^* = \frac{u_\infty}{A}\sin^{-1}\left[\frac{2A^2(u/u_\infty) - B}{(B^2 + 4A^2)^{1/2}}\right] \quad \textbf{Eq. 2}$$

where

$$A^2 = \frac{[(\gamma - 1)/2]\, M_\infty^2}{T_w/T_\infty} \quad \textbf{Eq. 3}$$

$$B = \frac{1 + [(\gamma - 1)/2]\, M_\infty^2}{T_w/T_\infty} - 1 \quad \textbf{Eq. 4}$$

and T_w/T_∞ is the ratio between wall and freestream temperatures. Maise and McDonald have shown that the proposed technique does not exhibit great sensitivity to the Mach number or Reynolds number, making it a suitable choice for normalization. A normalization of the boundary layer data to the model profile (κ=0.4, Π=0.5) is shown in Figure 26. For reference, a fit of the model to the data is also provided, shown in Figure 27.

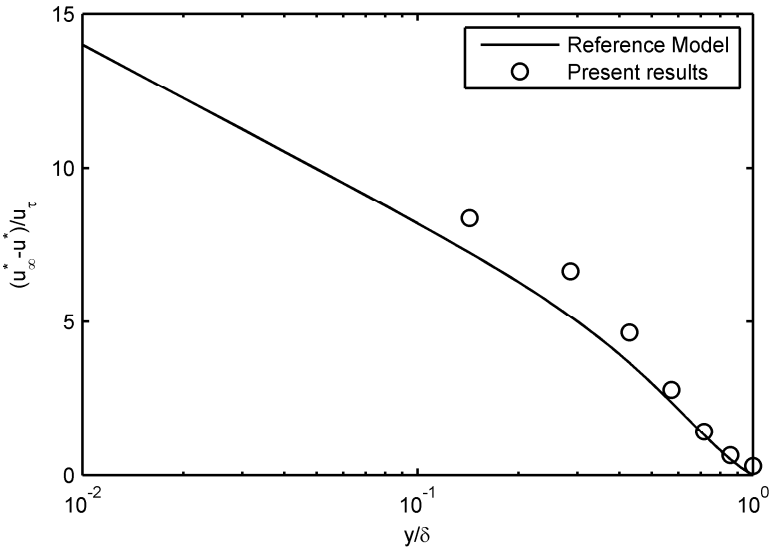

Figure 26. Comparison with turbulence model

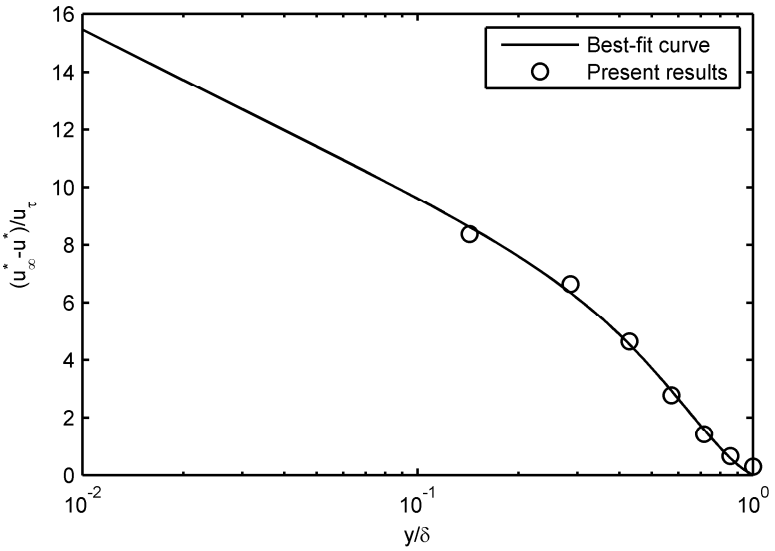

Figure 27. Turbulence model fit, u_τ = 43.8 m/s, Π = 0.789

It can be seen that the data and the turbulence model agree well with each other. The boundary layer data is in fair agreement with the Maise and McDonald reference model. In the upper region of the boundary layer, where the wake component dominates,

the agreement is excellent. Closer to the surface, where law of the wall dominates, the general trend is followed, but there is a discrepancy in the value of the normalized velocity. Performing a two-parameter curve fit of the model, yielding a friction velocity (u_τ) of 43.8 m/s and a skewness factor (Π) of 0.789, results in good overall agreement between the data and the fitted curve.

5.3 Surface Oil Flow Visualization

Surface oil flow visualization was performed on the shock impingement surface. A mixture of Titanium-White acrylic paint was mixed with SAE 85W-140 gear oil and applied thinly to the test section floor. The tunnel was then rapidly brought to its operating conditions: a stagnation pressure of 48 psig and a wedge angle of 8°. A deskewed image of the oil taken while the tunnel was running is shown in Figure 28. A top down image of the oil after a quick stop of the tunnel is shown in Figure 29.

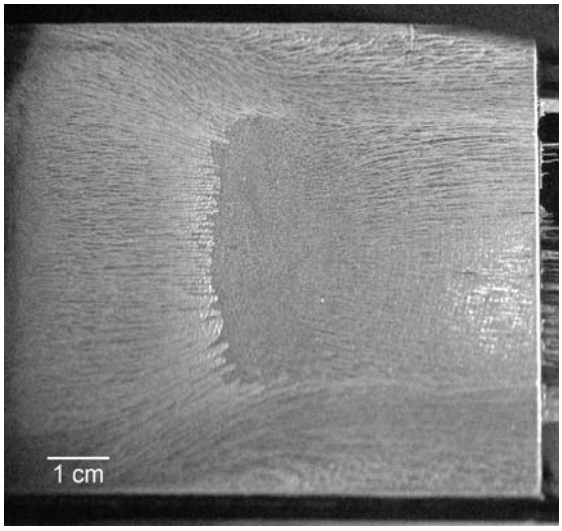

Figure 28.Deskewed oil flow visualization of active flow

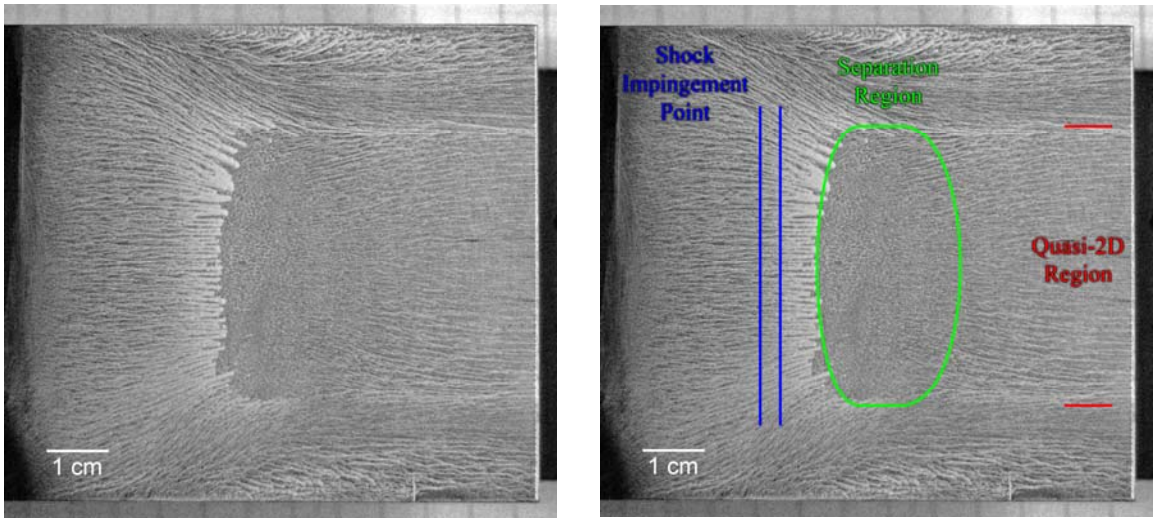

Figure 29. Surface oil flow visualization after settling

a) stock photograph; b) flow feature highlights

The advantage of performing surface oil flow visualization can be seen clearly. The onset of separation is relatively two-dimensional and spans about half the tunnel width about the centerline. On either side of the primary separation are sidewall separation regions. The reattachment point of the primary separation is bowed. The separation length, used as a normalization parameter elsewhere in this thesis, is about 20 mm measured along the centerline.

CHAPTER 6: SUMMARY AND FUTURE WORK

6.1 Summary

A new supersonic tunnel was designed and built for investigating supersonic inlet control using LAFPAs. A variable angle wedge served as the compression surface to generate the SWBLI. Placing the shock attachment point within the potential flow removed ceiling boundary layer turbulence from the incident shock unsteadiness. A linear actuator attached to the trailing edge of the wedge was used to vary the wedge angle and thereby the SWBLI strength.

Qualitative characterization of the flow was performed using schlieren imaging and surface oil flow visualization. Preliminary schlieren images revealed a separation region forming on the ceiling upstream of the wedge; this generated an interfering shock wave. After substantial troubleshooting, a thin wedge below a recessed ceiling in a higher Mach number flow resulted in adequate flow quality. Surface oil flow visualization revealed the size and shape of the separation region, which is thought to be the source of the reflected shock unsteadiness. The separation is notably three-dimensional, spanning only half the tunnel's width, but is essentially two-dimensional near the centerline.

Quantitative measurements were performed using stereoscopic PIV. The vector fields of the flow at two cross-stream planes show high quality data and clean flow. Boundary layer data at the upstream plane was averaged and used to plot the velocity

profile. The boundary layer profile was then normalized using the van Driest transformation and compared to profiles found in literature with good agreement.

6.2 Future Work

More work is required to fine-tune the facility. Clean flow will allow the effectiveness of the LAFPAs to be more accurately and conclusively determined. Modifications will also be made to the wedge design. A smaller and thinner wedge, which reduces flow obstruction, may eliminate any choking of the flow above the wedge and therefore remove the ceiling separation region entirely.

Further investigation of the SWBLI itself is also necessary, as its dynamics are not fully understood.[8] Flow control does not require an exact knowledge of the control mechanism, because control authority experiments can be performed over a wide parameter space to locate the optimum control parameters. However, increased understanding of the oscillation source and LAFPA control mechanism may allow for more intelligent design and placement of the actuators. Unsteady pressure measurements near and within the interaction region may yield more information about the SWBLI. Unsteady pressure measurements taken while the actuators are active may reveal useful information, but care must be taken so that the actuators do not arc to the pressure transducers.

The supersonic wind tunnel was built for investigating supersonic mixed compression inlet flow control using plasma actuators, so the actuators are to be investigated in detail. Many variables contribute to the control authority of the plasma actuators over a SWBLI. Those of most concern are: forcing frequency, streamwise

location, spanwise spacing, duty cycle, and mode of operation. Additionally the control authority of the LAFPAs is most likely dependent on interaction strength. To date, only the effects of frequency, streamwise location, and mode of operation on the LAFPA's control authority have been studied. The mode of operation has not been thoroughly investigated, as only two modes have been tested. A frequency sweep of the actuators including Strouhal numbers of 0.03 and 0.5 needs to be performed within the new tunnel; previous results suggest that a Strouhal number of 0.03 (the low-frequency unsteadiness present in the reflected shock of an unforced SWBLI) will yield the greatest control authority. In jet exhaust experiments, the LAFPAs have shown an increased effectiveness as the duty cycle is decreased (as long as complete breakdown occurs). The variable angle wedge allows for controllable interaction strength, so an investigation of the dependence of LAFPAs control authority on interaction strength is necessary.

Other investigative techniques should be employed to gain further insight into the SWBLI. Acetone planar laser scattering flow visualization, and smoke flow visualization can provide more qualitative information about the flow features. Specifically acetone and smoke visualization can be used to observe the separation region from a cross-stream point of view. Streamwise PIV would provide qualitative information from a different point of view, allowing the effect of actuation on the size of the separation bubble to be more readily observed. These techniques will allow for a better examination of the separation's size and shape, and possibly temporal evolution, than schlieren imaging due to the spanwise integration effect of schlieren. Time resolved streamwise PIV could be used to track the shock foot location. Synchronized streamwise PIV and unsteady pressure measurements may reveal critical correlations in the flow.

The proposed research will be performed in partial fulfillment of a Master of Science degree in Mechanical Engineering at The Ohio State University.

REFERENCES

1. Anderson, Bernhard H., Jon Tinapple, and Lewis Surber. "Optimal Control of Shock Wave Turbulent Boundary Layer Interactions Using Micro-Array Actuation." *AIAA Paper* 3rd Flow Control Conference 2006-3197 (2006): 1-14. Print.
2. Ogawa, H., and H. Babinsky. "Shock/Boundary-Layer Interaction Control Using Three-dimensional Bumps in Supersonic Engine Inlets." *AIAA 46th Aerospace Sciences Meeting and Exhibit*. Reno, Nevada, Jan. 7-10, 2008. 1-15. Vol. AIAA Paper. Print.
3. Kalra, Chiranjeev S., Sohail Zaidi, and Richard B. Miles. "Shockwave Induced Turbulent Boundary Layer Separation Control with Plasma Actuators." *AIAA Paper* 48th Aerospace Sciences Meeting and Exhibit 2008-1092 (2008): 1-8. Print.
4. Samimy, M., J. H. Kim, J. Kastner, I. Adamovich, and Y. Utkin. "Active Control of a Mach 0.9 Jet for Noise Mitigation Using Plasma Actuators." *AIAA Journal* 45 4 (2007): 890-901. Print.
5. Samimy, M., J.-H. Kim, J. Kastner, and I. Adamovich. "Noise Mitigation in High Speed and High Reynolds Number Jets Using Plasma Actuators." *AIAA/CEAS 13th Aeroacoustics Conference*, 2007. Vol. AIAA Paper. Print.
6. Samimy, M., J.-H. Kim, M. Kearney-Fischer, and A. Sinha. "Acoustic and Flow Fields of an Excited High Reynolds Number Axisymmetric Supersonic Jet." *Journal of Fluid Mechanics* 656 (2010): 507-529. Print.
7. Caraballo, E., N. Webb, J. Little, J. H. Kim, and M. Samimy. "Supersonic Inlet Flow Control Using Plasma Actuators." *AIAA Paper* 47th AIAA Aerospace Sciences Meeting 2009-924 (2009): 1-14. Print.
8. Dolling, David S. "Fifty Years of Shock-Wave/Boundary-Layer Interaction Research: What Next?" *AIAA Journal* 39 8 (2001): 1517-1531. Print.
9. Touber, Emile, and Neil D. Sandham. "Large-Eddy Simulation of Low-Frequency Unsteadiness in a Turbulent Shock-Induced Separation Bubble." *Theoretical and Computational Fluid Dynamics* 23 (2009): 79-107. Print.
10. Babinsky, H., Y. Li, and C. Pitt Ford. "Microramp Control of Supersonic Oblique Shock-Wave/Boundary-Layer Interactions." *AIAA Journal* 47 3 (2009): 668-675. Print.
11. Samimy, M., I. Adamovich, B. Webb, J. Kastner, J. Hileman, S. Keshav, and P. Palm. "Development and characterization of plasma actuators for high-speed jet control." *Experiments in Fluids* 37 4 (2004): 577-588. Print.
12. Webb, N. "Control of the Interaction Between an Oblique Shock Wave and a Supersonic Turbulent Boundary Layer by Localized Arc Filament Plasma Actuators." The Ohio State University, 2009. Print.

13. Utkin, Yurii G., Saurabh Keshav, Jin-Hwa Kim, Jeff Kastner, Igor V. Adamovich, and Mo Samimy. "Development and Use of Localized Arc Filament Plasma Actuators for High-Speed Flow Control." *Journal of Physics D: Applied Physics* 40 3 (2007): 685-694. Print.
14. Souverein, L., B. van Oudheusden, F. Scarano, and P. Dupont. "Application of a Dual-Plane Particle Image Velocimetry (dual-PIV) Technique for the Unsteadiness Characterization of a Shock Wave Turbulent Boundary Layer Interaction." *Measurement Science and Technology* 20 074003 (2009): 16. Print.
15. Beresh, S. "The Effect of the Incoming Turbulent Boundary Layer on a Shock-Induced Separated Flow using Particle Image Velocimetry." University of Texas, 1999. Print.
16. Ganapathisubramani, B., N. T. Clemens, and D. S. Dolling. "Effects of Upstream Boundary Layer on the Unsteadiness of Shock-Induced Separation." *Journal of Fluid Mechanics* 585 (2007): 369-394. Print.
17. Ganapathisubramani, B., N. Clemens, and D. Dolling. "Low-frequency Dynamics of Shock-Induced Separation in a Compression Ramp Interaction." *Journal of Fluid Mechanics* 636 (2009): 397-425. Print.
18. Humble, R., G. Elsinga, F. Scarano, and B. van Oudheusden. "Three-Dimensional Instantaneous Structure of a Shock Wave/Turbulent Boundary Layer Interaction." *Journal of Fluid Mechanics* 622 (2009): 33-62. Print.
19. Erengil, Mehmet Erdal, and D. S. Dolling. "Physical Causes of Separation Shock Unsteadiness in Shock Wave/ Turbulent Boundary Layer Interactions." *AIAA 24th Fluid Dynamics Conference*, 1993. Vol. AIAA Paper. Print.
20. Thomas, F. O., C. M. Putnam, and H. C. Chu. "On the mechanism of unsteady shock oscillation in shock wave/turbulent boundary layer interactions." *Experiments in Fluids* 18 (1994): 69-81. Print.
21. Ünalmis, Ö. H., and D. S. Dolling. "Experimental Study of Causes of Unsteadiness of SHock-Induced Turbulent Separation." *AIAA Journal* 36 (1998): 371-8. Print.
22. DuPont, P., C. Haddad, and J. F. Debie` ve. "Space and time organization in a shock-induced separated boundary layer." *Journal of Fluid Mechanics* 559 (2006): 255–277. Print.
23. Dupont, P., S. Piponniau, A. Sidorenko, and J. F. Debiéve. "Investigation by Particle Image Velocimetry Measurements of Oblique Shock Reflection with Separation." *AIAA Journal* 46 6 (2008): 1365-1370. Print.
24. Dussauge, Jean-Paul, Pierre Dupont, and Jean-Francois Debiève. "Unsteadiness in Shock Wave Boundary Layer Interactions with Separation." *Aerospace Science and Technology* 10 2 (2006): 85-91. Print.
25. Piponniau, S., J. P. Dussauge, J. F. Debiève, and P. DuPont. "A Simple Model for Low Frequency Unsteadiness in Shock Induced Separation." *Journal of Fluid Mechanics (under consideration)* N/A N/A (2009): N/A. Print.
26. Touber, Emile, and Neil D. Sandham. "Comparison of Three Large-Eddy Simulations of Shock-Induced Turbulent Separation Bubbles." *Springer* (2009). Print.

27. Pirozzoli, S., and F. Grasso. "Direct numerical simulation of impinging shock wave/turbulent boundary layer interaction at M=2.25." *Physics of Fluids A* 18 (2006): 1-17. Print.
28. Yan, H., and D. Gaitonde. "Effect of Thermally-Induced Surface Perturbation in Compressible Flow." *AIAA Paper* 47th AIAA Aerospace Sciences Meeting 2009-0923 (2009): 1-16. Print.
29. Settles, G. S. *Schlieren and Shadowgraph Techniques: Visualizing phenomena in Transparent Media*. Experimental Fluid Mechanics. Eds. R. Adrian, et al. New York: Springer, 2001. Print.
30. Maise, George, and Henry McDonald. "Mixing Length and Kinematic Eddy Viscosity in a Compressible Boundary Layer." *AIAA Journal* 6 1 (1968): 73-80. Print.